Evidence for the Two Phosphate Binding Sites of an Analogue of the Thioacyl Intermediate for the *Trypanosoma cruzi* Glyceraldehyde-3-phosphate Dehydrogenase-Catalyzed Reaction, from Its Crystal Structure†

Marcelo S. Castilho, Fernando Pavão, and Glaucius Oliva‡

Instituto de Física de São Carlos, USP, P.O. Box 369, 13560-970 São Carlos, SP, Brazil

Sylvain Ladame, Michèle Willson,‡ and Jacques Périé*,‡

Laboratoire de Synthèse et de Physico Chimie de Molécules d'Intérêt Biologique UMR-CNRS 5068, Groupe de Chimie Organique Biologique, Université Paul Sabatier, 118, route de Narbonne, 31062 Toulouse Cedex, France

Received October 3, 2002; Revised Manuscript Received March 31, 2003

ABSTRACT: Glyceraldehyde-3-phosphate dehydrogenase (GAPDH) catalyzes the reversible oxidative phosphorylation of D-glyceraldehyde 3-phosphate (GAP) into D-glycerate 1,3-bisphosphate (1,3-diPG) in the presence of NAD^+ and inorganic phosphate (P_i). Within the active site, two anion-binding sites were ascribed to the binding of the C3 phosphate of GAP (P_s) and to the binding of the attacking phosphate ion (P_i). The role played by these two sites in the catalytic mechanism in connection with the functional role of coenzyme exchange (NADH−NAD^+ shuttle) has been investigated by several studies leading to the C3 phosphate flipping model proposed by Skarzynski et al. [Skarzynski, T., Moody, P. C., and Wonacott, A. J. (1987) *J. Mol. Biol. 193*, 171−187]. This model has not yet received direct confirmation. To gain further insight into the role of both sites, we synthesized irreversible inhibitors which form with the essential cysteine residue a thioacyl enzyme analogue of the catalytic intermediate. Here we report the refined glycosomal *Trypanosoma cruzi* GAPDH in complex with a covalently bound GAP analogue at an improved resolution of 2.0−2.5 Å. For this holo-thioacyl enzyme complex, a flip-flop movement is clearly characterized, the change from the P_i to the P_s binding site being correlated with the coenzyme exchange step: the weaker interaction of the intermediate when bound at the P_s site with the cofactor allows its release and also the binding of the inorganic phosphate for the next catalytic step. This result gives strong experimental support for the generally accepted flip-flop model of the catalytic mechanism in GAPDH.

Glyceraldehyde-3-phosphate dehydrogenase (GAPDH), the sixth enzyme in the glycolytic pathway, has been widely studied for its central role in energy production in both prokaryotes and eukaryotes. Additionally, intense research over the past decade has provided new insights into the functional diversity of mammalian GAPDH, more precisely its involvement in membrane transport, nuclear RNA externalization, transcriptional control of gene expression, and DNA replication and repair (*1*). More recently, it was shown that GAPDH plays important roles in apoptosis (*2*), in neuronal disorders (*3*−*5*), and in certain types of cancer (*6*). Despite the involvement of GAPDH in such a variety of biological functions, this enzyme has an essential role in the control of glycolytic metabolite flux (*7*). So, GAPDH has been identified as a suitable target for the development of inhibitors of glycolysis in parasites of the Trypanosomatidae family (*8*). More specifically, *Trypanosoma cruzi*, the causative agent of Chagas disease in South-America, is highly dependent on glycolysis in infectious stages in mammals (*9*). From the mechanistic and structural results described here, a family of irreversible inhibitors is proposed as a set of lead compounds for the development of news drugs against Chagas disease.

GAPDH catalyzes the oxidative phosphorylation of glyceraldehyde 3-phosphate (GAP)[1] into 1,3-bisphospho-D-glyceric acid (1,3-diPG) with the involvement of inorganic phosphate (P_i) and nicotinamide adenosine dinucleotide (NAD^+). Its dehydrogenase activity depends on the [NAD^+]/[NADH] ratio, which needs to be kept constant in the cell. The reaction mechanism has been intensively investigated (*10*−*12*) and the multistep catalytic process, proposed in 1976 (*13*), can be decomposed as follows: (i) an oxido-reduction reaction, corresponding to the nucleophilic attack of an activated cysteine on the carbonyl group of GAP, followed by a hydride transfer from the generated thiohe-

† This work was done within the Comité Français d'Evaluation de la Coopération Universitaire avec le Brésil (COFECUB) program (Contract 294 H99) which is fully acknowledged.

* To whom correspondence should be addressed. E-mail: perie@cict.fr. Fax: (33) 5 61 55 60 11.

‡ Main authors.

[1] Abbreviations: gGAPDH, glycosomal D-glyceraldehyde-3-phosphate dehydrogenase (EC 1.2.1.12); GAP, glyceraldehyde 3-phosphate; P_i, inorganic phosphate; P_s, phosphate group of the substrate glyceraldehyde 3-phosphate; 1,3-diPG, 1,3-bisphosphoglycerate; NADH, nicotinamide adenine dinucleotide (reduced form); NAD^+, nicotinamide adenine dinucleotide (oxidized form); EDTA, ethylenediaminetetraacetic acid; NMR, nuclear magnetic resonance; MS, mass spectra; FTIR, Fourier transform infrared; DTT, dithiothreitol.

10.1021/bi0206107 CCC: $25.00
Published on Web 05/22/2003

miacetal to NAD^+, leading to the formation of a thioacyl enzyme, and (ii) a phosphorylation of the resulting thioester through the nucleophilic attack of inorganic phosphate on the carbonyl of the thioacyl group which leads to the formation of 1,3-diPG, which is subsequently released from the active site.

The three-dimensional structures of GAPDHs from several organisms have been crystallographically determined (*14*−*22*, *41*). A common feature of these structures is the presence of two highly conserved cationic sites which were identified in the GAPDH active site and are able to bind two sulfate or phosphate ions in each monomer. On the basis of modeling studies, these cationic sites were assumed to be the two phosphate binding sites; P_s is the C3 phosphate of GAP and P_i the inorganic phosphate. Although they were initially considered as specific interaction sites of each substrate, Skarzynski et al. (*16*) later established a more complex mechanism involving the possible transfer of the C3 phosphate of GAP from one site to the other during the sequence of catalytic events. From these earlier studies, it was proposed that the C3 phosphate of GAP should initially interact with the P_i site during the steps leading to the formation of the acyl enzyme intermediate. The coenzyme exchange step is thought to result from a conformational isomerization of the thioacyl enzyme intermediate of the C3 phosphate of GAP from the P_i to the P_s site. The now free P_i site could then bind inorganic phosphate, and the phosphorylation on C_1 could then proceed by nucleophilic attack. Although Corbier et al. (*23*) have shown, by site-directed mutagenesis and kinetic studies, that the C3 phosphate of GAP first interacts at the P_i site, flipping toward the P_s site has never been demonstrated. Moreover, recent studies have suggested that this GAP phosphoryl group could also interact with a third cationic site, slightly different from the P_i site and called the "new P_i site" (*20*). Finally, more recent results of Yun et al. (*24*) obtained with the hemiacetal intermediate of *Escherichia coli* GAPDH are also in accordance with the flip-flop model. However, they do not provide direct evidence of this process. To shed some light on these mechanistic aspects, we thought that it would be helpful to mimic as closely as possible the acyl enzyme intermediate. Indeed, the three-dimensional structure of the enzyme−substrate−cofactor ternary complex could reveal the detailed binding modes of the substrate, allowing the evaluation of (1) the contribution made by phosphate binding sites and (2) the functional role of coenzyme exchange in the catalytic process. The formation of a thioacyl enzyme analogue could be obtained through the reaction between the active site cysteine residue and an activated carbonyl group of a GAP analogue, leading to an irreversibly bound and therefore stable complex. The previously described irreversible GAPDH inhibitors that are covalently bound at the active cysteine residue (*25*−*30*) are not good representatives of the thioacyl enzyme intermediate.

We report here the synthesis of (*p*-nitrophenoxycarboxyl)propyl dihydroxyphosphonates, as GAP analogues, and their inactivation effects on glycosomal *T. cruzi* GAPDH (gGAPDH), in the search for compounds that covalently bind to the cysteine residue of the enzyme to produce a thioester complex. We also present the crystal structure of the holothioacyl enzyme complex of *T. cruzi* GAPDH with one member of this family of compounds, which reveals that the phosphoryl group of the molecule interacts with both P_i and P_s sites. Comparison of this complex with the holoenzyme from *T. cruzi* shows that a conformational change of the protein is induced upon inhibitor binding. Detailed analysis of interactions between the substrate analogue, cofactor, and protein provides strong experimental support for the generally accepted catalytic mechanism.

MATERIALS AND METHODS

Synthesis of Inhibitors. All chemical reagents were purchased form either Aldrich or Lancaster Co. The pure compounds were identified by spectrometric analysis on an apparatus of the Institute at Molecular Chemistry Paul Sabatier (ICMPS-IR1744). IR spectra were recorded on a Perkin-Elmer FTIR 1610 spectrometer; ^1H, ^{13}C, and ^{31}P NMR spectra were recorded on Bruker 250 and 200 MHz FT apparatus, and mass spectra were determined on a Nemag R10-10 spectrometer. Elemental analysis was performed at the INP-ENSCT on an Eager 200 apparatus.

Synthesis of Carboxylic Acids. 4-(Diethoxyphosphoryl)-butanoic acid **1a** and 4-(diethoxyphosphoryl)-2-butenoic acid **2a** were prepared by saponification of their corresponding ethyl esters and then isolated in their acidic form (Supporting Information). 2-[2-(Diethoxyphosphoryl)ethyl]acrylic acid **3a** was prepared by condensation of the carbanion of diethylmethyl phosphonate on 3-bromo-2-(bromoethyl)propanoic acid via a double addition−elimination reaction. To a solution of diethylmethyl phosphonate (1.47 g, 9.7 mmol) in anhydrous THF (20 mL) was slowly added 7.3 mL of *n*-BuLi (11.6 mmol) at −78 °C. After being stirred for 15 min at −78 °C, this solution was added, via a cannula, to a solution of 3-bromo-2-(bromoethyl)propanoic acid (1.18 g, 4.8 mmol) and *n*-BuLi (3.4 mL, 5.3 mmol) in anhydrous THF (15 mL) at −78 °C. After being stirred for 1 h at −78 °C and overnight at room temperature, the mixture was neutralized with an aqueous solution saturated with NH_4Cl and then acidified to pH 4 with a 1 M HCl solution. The aqueous layer was subsequently extracted with CH_2Cl_2 (3 × 50 mL), and the organic layer was dried with $MgSO_4$, filtered, and evaporated. After purification by flash chromatography (95:5 CH_2Cl_2/MeOH, and then 90:10), compound **3a** was obtained as a pure colorless oil (0.71 g, 58%): ^1H NMR (250 MHz, $CDCl_3$) δ 1.2 (m, 6H), 1.8−2.0 (m, 2H), 2.4−2.5 (m, 2H), 3.9−4.0 (m, 4H), 5.5 (s, 1H), 6.1 (s, 1H), 11.4 (s, 1H); ^{13}C NMR (62.9 MHz, $CDCl_3$) δ 16.2 (d, J_{C-P} = 6.2 Hz), 24.4 (d, J_{C-P} = 140.8 Hz), 25.1 (d, J_{C-P} = 3.9 Hz), 61.9 (d, J_{C-P} = 6.5 Hz), 126.1, 139.5 (d, J_{C-P} = 17.5 Hz), 169.0; MS (DCI, NH_3) *m*/*z* 237 (MH^+), 254 (MNH_4^+).

Synthesis of p-Nitrophenyl Esters. They were prepared from the corresponding carboxylic acids by addition of *p*-nitrophenate anion on the nonisolated acyl chloride intermediate (**1b** and **2b** in the Supporting Information). For compound **3b**, to a solution of carboxylic acid (10 mmol) in anhydrous CH_2Cl_2 (20 mL) was added thionyl chloride (1.1 mL, 15 mmol). After the mixture had been stirred overnight at room temperature, the volatile components were evaporated off, leading to the pure expected acid chloride evidenced by IR spectroscopy ($\nu_{C=O}$ = 1747 cm^{-1}). The oily residue was then dissolved in anhydrous CH_2Cl_2 (20 mL), and a solution of *p*-nitrophenol (1.26 g, 9.1 mmol) and anhydrous triethylamine (1.55 mL, 11.2 mmol) in CH_2Cl_2

(20 mL) was slowly added at 0 °C. After the mixture had been stirred for 3 h at room temperature, the triethylammonium salts were filtered off, and the organic layer was washed with an aqueous solution saturated with NaCl (50 mL), dried with $MgSO_4$, filtered, and evaporated. *p*-Nitrophenyl ester **3b** was thus obtained as a pale yellow oil (98% yield).

3-(*p*-Nitrophenoxycarboxyl)-3-ethylene propyl diethylphosphonate **3b**: ^{1}H NMR (250 MHz, $CDCl_3$) δ 1.3 (t, 6H, J_{H-P} = 7.1 Hz), 1.9−2.0 (m, 2H), 2.6−2.7 (m, 2H), 4.0−4.1 (m, 4H), 5.8 (s, 1H), 6.4 (s, 1H), 7.2 (d, 2H, J_{H-H} = 9.1 Hz), 8.2 (d, 2H, J_{H-H} = 9.1 Hz); ^{13}C NMR (62.9 MHz, $CDCl_3$) δ 16.4 (d, J_{C-P} = 6.1 Hz), 24.5 (d, J_{C-P} = 141.6 Hz), 25.4 (d, J_{C-P} = 3.8 Hz), 61.6 (d, J_{C-P} = 6.5 Hz), 122.5, 125.2, 128.7, 138.2 (d, J_{C-P} = 16.7 Hz), 145.3, 155.4, 163.9; ^{31}P NMR (81 MHz, $CDCl_3$) δ 30.3; MS (DCI, NH_3) *m*/*z* 358 (MH^+), 375 (MNH_4^+).

Synthesis of Dihydroxyphosphonates. They were prepared by following a classical procedure using bromotrimethylsilane (**1c** and **1b** in the Supporting Information**)**. For **3c**, bromotrimethylsilane (2.1 mL, 15.4 mmol) was added to diethyl phosphonate **3b** (3.9 mmol) stored under an argon atmosphere. After the mixture had been stirred for 6 h at room temperature, all volatile components were removed by evaporation, and the oily residue was dissolved in Et_2O (15 mL) and extracted with water (30 mL). **3c** was obtained pure as a white or pale yellow powder (95% yield) after the aqueous solution had been freeze-dried.

3-(*p*-Nitrophenoxycarboxyl)-3-ethylene propyl dihydroxyphosphonate **3c**: ^{1}H NMR (250 MHz, D_2O) δ 2.0−2.1 (m, 2H), 2.6−2.7 (m, 2H), 6.0 (s, 1H), 6.5 (s, 1H), 7.4 (d, 2H, J_{H-H} = 9.1 Hz), 8.3 (d, 2H, J_{H-H} = 9.1 Hz); ^{13}C NMR (62.9 MHz, D_2O) δ 27.4 (d, J_{C-P} = 3.4 Hz), 27.9 (d, J_{C-P} = 135.5 Hz), 125.4, 128.1, 132.3, 140.3 (d, J_{C-P} = 16.1 Hz), 148.0, 157.9, 169.0; ^{31}P NMR (81 MHz, D_2O) δ 30.6. Anal. Calcd for $C_{11}H_{12}NO_7P$ (301): C, 43.87; H, 4.02; N, 4.65. Found: C, 44.01; H, 3.86; N, 4.72.

Enzyme Inhibition Assays. Assay reactions (total volume of 1.0 mL) were carried out at 25 °C in a 100 mM triethanolamine, HCl buffer (pH 7.5, I = 0.15) containing 1 mM EDTA, 0.1 M KCl, 10 mM K_2HPO_4, 2 mM NAD^+, 0.8 mM GAP, 20 μL of a glyceraldehyde-3-phosphate dehydrogenase-containing solution, and variable concentrations of the inhibitor. The remaining GAPDH activity was determined by following at 340 nm the formation kinetics of NADH resulting from the reduction of NAD^+ by the enzyme. In all cases, the rates are expressed in micromoles of product formed per minute. One enzyme unit is defined as the amount of enzyme necessary for the formation of 1 μmol of 1,3-diPG/min.

For irreversible inhibitors, the inactivation kinetics were established by using saturating conditions of substrates and cofactor, after incubation of the enzyme with at least five different concentrations of inhibitor (5, 15, 25, 50, and 75 μM). Experiments were carried out in triplicate, and individual initial rates were kept only when they corresponded to values obtained with correlation coefficients equal to or better than 0.998. The percentage of remaining activity was determined with respect to a reference, the enzyme incubated without inhibitor during the same period of time.

Preparation and Purification of Glycosomal T. cruzi GAPDH. Recombinant *T. cruzi* gGAPDH was prepared and purified according to the previously reported procedure (*22*) with minor modifications. No DTT was used in the purification buffer since it can react with the inhibitors.

Table 1: Collection and Processing Statistics

oscillation angle	1.0°
total no. of frames	134
total no. of collected reflections	134297
no. of unique reflections	48450
resolution range	20.0−2.5 Å
overall completeness	99.0% (97.5%)[a]
overall R_{merge}	11.3% (43.8%)[a]
$I/\sigma I$	9.7 (2.6)[a]
redundancy	2.8 (2.5)[a]

[a] The values in parentheses correspond to the last resolution shell (2.56−2.5 Å).

Cocrystallization Assays. Cocrystallization assays were carried out using a protein solution at 10 mg/mL and NAD^+ at a saturating concentration, preincubated with 2.0 mM inhibitor. Crystals of the gGAPDH−3-(*p*-nitrophenoxycarboxyl)-3-ethylene propyl dihydroxyphosphonate (**3c**) complex were grown at 18 °C by hanging drop vapor diffusion, against a reservoir solution of 0.1 M sodium cacodylate buffer (pH 7.3−7.5), with 0.1 M calcium acetate, 18% polyethylene glycol 8000, 1.0 mM EDTA, and 1.0 mM sodium azide. The hanging drops were set up with equal volumes (5 + 5 μL) of gGAPDH solution and reservoir buffer. Small flat crystals appeared within 2 weeks.

Data Collection and Processing. A single crystal of the gGAPDH−**3c** complex was flash-cooled to 100 K in an Oxford Cryostream Cooler. The cryoprotectant solution that was used consisted of 20% polyethylene glycol 400 added to the reservoir solution described above. Monochromatic X-ray data collection was performed in the Brazilian National Synchrotron Light Laboratory (LNLS) (*31*), using an incident wavelength of 1.54 Å. Diffraction spots were recorded on a MAR345 image plate, using the rotation method (*32*). Data indexing and scaling were carried out with DENZO and SCALEPACK, respectively (*33*). Data collection and processing statistics are summarized in Table 1. The collected crystal belonged to space group $P2_1$ with the following unit cell parameters: a = 81.46 Å, b = 85.26 Å, c = 105.15 Å, and β = 95.61°. The analysis of crystal contents reveals one tetramer per asymmetric unit and a V_m value of 2.21 Å^3/Da.

Structure Determination and Refinement. The structure was determined by molecular replacement, using AMoRe (*34*). The native tetrameric gGAPDH structure (*22*) without cofactor and water molecules was used as a search model. Further refinement was performed using the CNS programs (*35*) with torsional molecular dynamics and maximum likelihood functions, and the addition of water molecules was conducted with ARP (*36*). Manual rebuilding of the macromolecular model and graphic visualization were performed using O (*37*). The crystallographic R_{factor} and R_{free} values, as well as the stereochemical quality of the model, were constantly monitored during the course of the refinement with PROCHECK (*38*). AMoRe provided a clear solution with one tetramer in the asymmetric unit, with a correlation factor of 0.67 and an R_{factor} of 0.33. The rotated and translated model was refined with a simulated annealing protocol using noncrystallographic symmetry (NCS) restraints. This refinement produced an R_{factor} of 0.33 and an R_{free} of 0.34. Visual analysis of $F_o - F_c$ and $2F_o - F_c$ maps revealed clear electron density for the NAD cofactor only in monomer D.

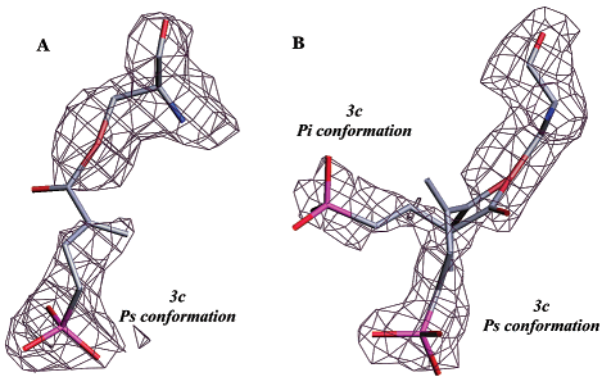

FIGURE 1: $2F_o - F_c$ map contoured at 0.8δ in the active site of monomer D, represented in panel A (P_s conformation), and monomer B, represented in panel B (P_s and P_i alternate conformations). The continuous electron density from Cys166 to **3c** supports its covalent binding in both conformations, as discussed above. Atoms are colored according to the following code: C atoms in light purple, N atoms in blue, S atoms in orange, P atoms in pink, and O atoms in red. This figure was created in O (*37*).

This molecule was included, and a new refinement cycle was performed, without NCS restraints. R_{factor} decreased to 0.23 and R_{free} to 0.29. After several cycles of manual rebuilding with O and minimization steps, unequivocal density for the inhibitor could be clearly identified in the active site of monomer D (Figure 1A). One molecule of **3c** was manually built into this density, and water molecules were automatically added to the model using the program ARP. The refinement cycles resulted in an R_{factor} of 0.20 and an R_{free} of 0.27. Careful analysis of the electron density maps indicated that subunits B and C could also have both NAD and inhibitor bound, possibly with lower occupancies. Therefore, NAD and the inhibitor were added to the atomic model, in the same conformation that was found in monomer D, and the subsequent refinement cycle included their occupancies as parameters, which converged to approximately 50%. At this point, a difference Fourier map showed density close to Cys166 in monomers B and C, in which the inhibitor **3c** could be fitted, in an alternative conformation (Figure 1B). As the previous refinement had shown half-occupancy for the first conformation, an identical value (50%) was assigned to the occupancy of the second conformation.

In the first conformation, the phosphonate moiety is located at the P_s binding site, and in the second conformation, it occupies the P_i binding site. The final cycles of refinement included as the atomic model the four protein subunits (named A−D), one NAD molecule and one inhibitor **3c** in the P_s conformation in subunit D, one NAD molecule and two alternative conformers of **3c** in subunits B and C, and a total of 695 water molecules. All amino acid side chains which did not exhibit any electron density in the final maps were assigned zero occupancies. The final crystallographic results are summarized in Table 2.

Table 2: Final Refinement Statistics

resolution range	20.0−2.5 Å
no. of amino acid residues per monomer	359
no. of water molecules in the asymmetric unit	695
no. of inhibitor molecules	three (one in monomer B with two alternative conformations, one in monomer C with two alternative conformations, and one in monomer D in only one conformation)
R_{factor}	0.20
$R_{free,3\%}$	0.26
rms deviation for bonds	0.0063 Å
rms deviation for angles	1.22°

RESULTS

Design and Synthesis of GAPDH Inhibitors. It was previously shown that GAPDH is a good target for the design of irreversible inhibitors since its mechanism involves the formation of a covalent intermediate between the enzyme and the substrate GAP. Following the strategy of targeting the cysteine residue of the GAPDH active site involved in this covalent bonding, a few compounds bearing a reactive electrophilic site such as an epoxide or an α-enal were synthesized and proved to be potent GAPDH irreversible inhibitors (*29*). Since all these inhibitors bind to this cysteine residue through the formation of a thioether or an unstable thiohemiacetal linkage, we decided to design stable GAP analogues by replacing the aldehyde group in the inhibitor with an activated ester. We describe here the synthesis of three phosphonates, which are much less sensitive to hydrolysis than their phosphate analogues. The compounds were designed to bear a *p*-nitrophenol ester group, chosen to react with the active site cysteine to form a thioacyl enzyme, analogous to that formed during the catalytic mechanism. In this reaction, the *p*-nitrophenate group is released and can be easily monitored by its typical absorption at 410 nm. Schemes depicting the syntheses of compounds **1c**, **2c**, and **3c** are given in the Supporting Information. These *p*-nitrophenyl esters were synthesized from the corresponding carboxylic acids via the formation of an acyl chloride intermediate. The phosphoric ethoxy ester protecting groups were removed in the last step by hydrolysis of instable trimethylsilyl phosphoric ester intermediates.

Irreversible Inhibition of GAPDH. The three *p*-nitrophenol esters **1c**−**3c**, which are GAP analogues, give a time-dependent inactivation of *T. cruzi* gGAPDH. The saturated derivative **1c** proved to be too unstable to allow the determination of the corresponding inhibition constants. Consequently, we focused our study on compounds **2c** and **3c**, which are much more stable because of the presence of a conjugated unsaturated group. Inactivation of *T. cruzi* gGAPDH by compound **3c** follows pseudo-first-order kinetics. This irreversible effect was confirmed by the fact that no enzymatic activity was recovered after dilution of the enzyme/inhibitor mixture obtained after the incubation time. The plot of the reciprocal of the inactivation half-life versus inhibitor concentration results in a straight line passing through the origin, the slope of which corresponds to the k_{second} value. *T. cruzi* gGAPDH was inactivated by compound **3c** 6 times faster than with compound **2c** since the k_{second} values are 7000 and 1200 M^{-1} min^{-1}, respectively. The kinetic equation describing this pathway under steady state conditions is expressed according to the classical kinetic expression (*39*).

Interaction Mode. Since these irreversible inhibitors bear a Michael acceptor, two different ways of inactivation were possible. In the first (Scheme 1A), addition of the thiol of

Scheme 1: Two Possible Inactivation Paths of GAPDH by Inhibitor **3c**[a]

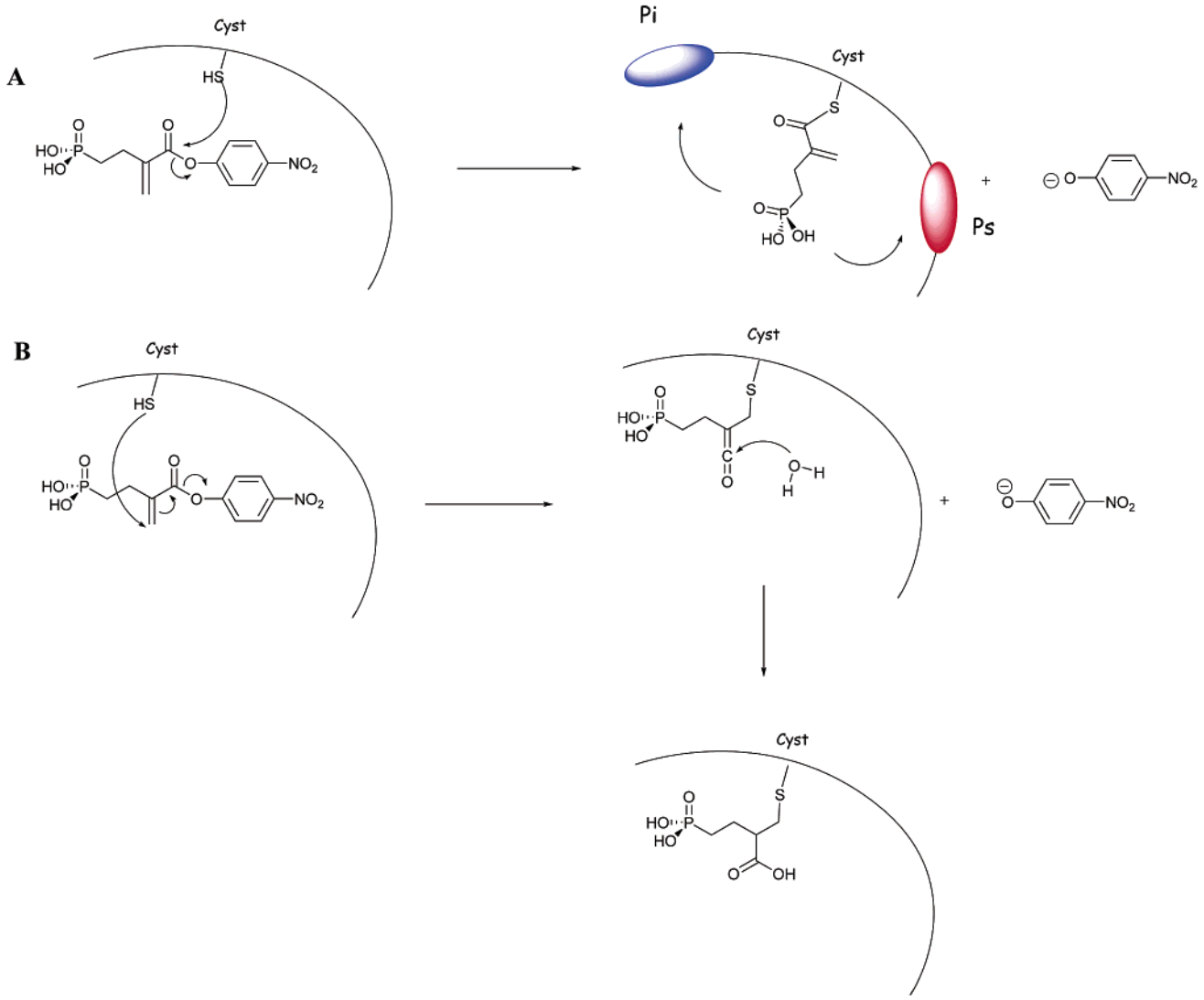

[a] (A) Nucleophilic attack on the carbonyl group and (B) 1,4-nucleophilic addition.

the cysteine residue on the carbonyl group could lead to the expected thioacyl enzyme that mimics the covalent intermediate formed with GAP. In a second (Scheme 1B), a 1,4-addition on the conjugated ethylenic system could lead to an enzyme−inhibitor covalent complex through the formation of a thioether bond. This configuration would not only enable the analysis of the specific interactions between *T. cruzi* gGAPDH and this series of inhibitors but also provide complementary information about the GAPDH reaction mechanism. To elucidate this question, X-ray analysis of the complex was undertaken.

Quality of the Structure. The structure has good stereochemistry indicators, with more than 99% of the residues showing main chain torsional angles in the allowed regions of the Ramachandran plot (*40*). Only Val255 is in an unfavorable region, though conserved in all other available GAPDH structures (*14*, *16*, *17*, *20*, *22*). This residue is in a loop between two consecutive β-strands, in a conformation considered to be important for maintaining the correct positioning of the active residue Cys166 with respect to the nicotinamide ring of the NAD^+ cofactor during catalysis. The average temperature factor values for the main chain atoms and all atoms of the 359 residues from each monomer are as follows: 25.11 and 24.65 Å^2 for monomer A, 31.07 and 30.53 Å^2 for monomer B, 42.74 and 42.50 Å^2 for monomer C, and 23.70 and 23.22 Å^2 for monomer D, respectively. The higher *B*-factor in monomer C reflects its higher mobility in the crystal lattice. Indeed, careful analysis of the crystal contacts of each of the four monomers in the a.u. indicates that subunit A has four neighboring monomers, subunit B has six neighboring monomers, subunit D has four neighboring monomers, and finally subunit C has only one neighboring monomer in the lattice, and this contact is made through the catalytic domain that forms the core of the tetrameric particle which is conformationally conserved in all four subunits.

*Interactions of Compound **3c** with the Protein.* The inhibitor is clearly bound to Cys166 and forms a thioester resulting from the nucleophilic attack of the thiol on the activated ester carbonyl group. The inhibitor is found in two alternative conformations (Figure 1B), hereafter named the "P_s conformation", present in monomers B−D, and the "P_i conformation", present only in monomers B and C. In the P_i conformation, the **3c** phosphoryl group hydrogen bonds to residues Thr226 and Arg249 and its phosphorus atom is 3.35 Å from the previous position described for the phosphate

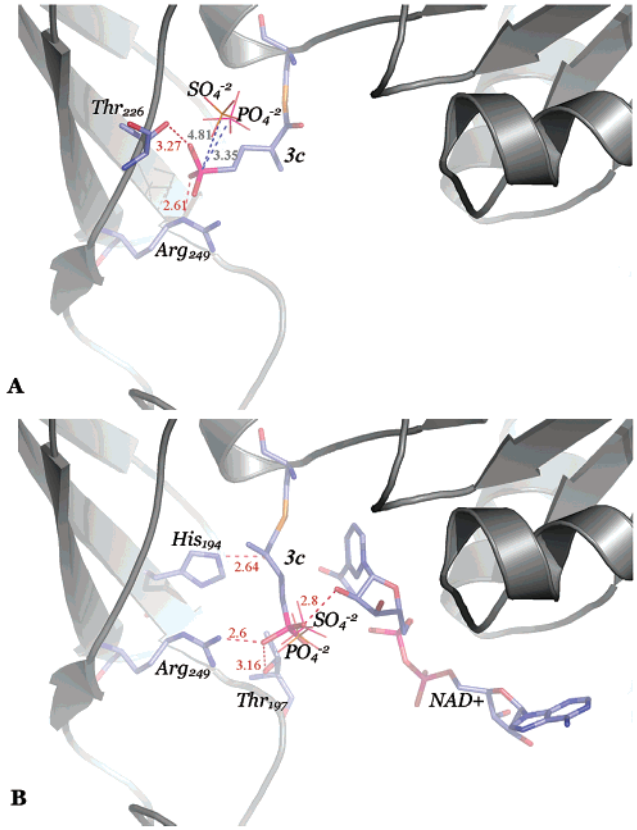

FIGURE 2: (A) Interaction profile of **3c** in the P_i binding site. The phosphoryl moiety, which is displaced 3.35 Å from the previously reported position of *L. mexicana* PO_4^{2-} and 4.81 Å from the previously reported position of *T. brucei* SO_4^{2-} (blue dashed lines), hydrogen bonds to residues Thr226 and Arg249 (red dashed lines). (B) Interaction profile of **3c** in the P_s binding site. The phosphoryl moiety hydrogen bonds to residues Thr197, His194, and Arg249 (red dashed lines). *L. mexicana* PO_4^{2-} and *T. brucei* SO_4^{2-} binding positions are also depicted. In a comparison of panels A and B of Figure 2, it becomes clear that the P_s binding site has a much more strict position. In fact, the **3c** phosphoryl moiety is only 0.93 Å from the previously reported position of *L. mexicana* PO_4^{2-} and 0.70 Å from the previously reported position of *T. brucei* SO_4^{2-}, not represented for reasons of clarity. Protein structure is presented in cartoon representation, apart from residues Thr197, His194, Thr226, and Arg249 that have all atoms represented. *L. mexicana* PO_4^{2-} and *T. brucei* SO_4^{2-} atoms come from crystallographic superposition of 1GYP and 1A7K on the **3c**−gGAPDH structure. This figure was created in Pymol.

binding site in *Leishmania mexicana* gGAPDH (*41*) and 4.81 Å from the sulfate binding site in *Trypanosoma brucei* gGAPDH (*17*) (Figure 2A). In this conformation, the **3c** carbonyl group points to the positively charged NAD^+ nicotinamide ring with the distance between O_1 of **3c** and N_1 of NAD^+ being 3.63 Å, longer than the usual length of the charge interaction predicted by Yun et al. (*24*).

In the P_s conformation, the **3c** phosphoryl group, which is located 0.93 Å from the previous position described for the inorganic phosphate binding site in *L. mexicana* gGAPDH (*41*) and 0.70 Å from the sulfate binding site in *T. brucei* gGAPDH (*17*), hydrogen bonds to residues Thr197 and Arg249 and to the C2′-hydroxyl group of the ribose sugar of the cofactor (Figure 2B). In addition, its carbonyl group hydrogen bonds to His194. Similar interactions should be present when the thioketal intermediate binds in the P_s conformation. It should be stressed that in this conformation

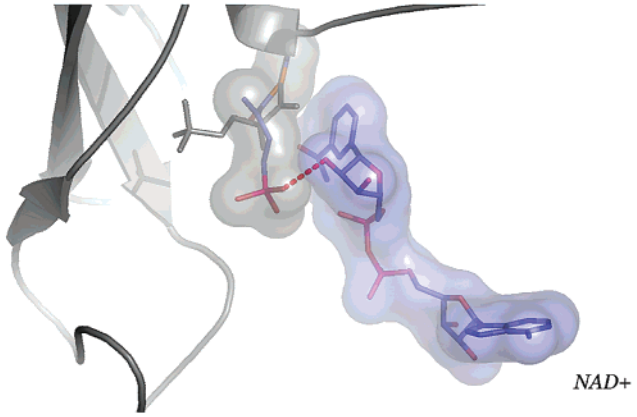

FIGURE 3: Interaction profile of **3c** with NAD. When bonded in the P_s conformation, the **3c** phosphoryl moiety hydrogen bonds to NAD's ribose, which is 2.83 Å from it. In fact, this interaction together with hydrophobic contacts between **3c** and NAD, represented by surface complementarity, is supposed to hold the cofactor in place. When bonded in the P_i conformation (gray), **3c** loses these interactions to NAD. Protein structure is represented as a gray cartoon, and NAD and **3c** are represented in sticks colored according to the following code: C atoms in light purple, N atoms in blue, S atoms in orange, P atoms in pink, and O atoms in red. This figure was created in Pymol.

Table 3: Comparison of the rms Differences (Å) in the Superposition of Cα Atoms from Equivalent Domains in Each Pair of Subunits in the Enzyme[a]

		catalytic domain			
		subunit A	subunit B	subunit C	subunit D
coenzyme binding domain	subunit A		0.57	0.82	0.73
	subunit B	0.21		0.79	0.69
	subunit C	0.19	0.21		0.74
	subunit D	0.20	0.22	0.18	

[a] The catalytic domain is formed by residues 151−330, and the NAD binding domain is formed by residues 1−150 at the N-terminus and residues 331−359 at the C-terminus.

the carbonyl group points away from the positively charged nitrogen of the nicotinamide moiety (Figure 3), once more excluding the possibility of charge interaction between **3c** and NAD^+.

Overall Structures. The monoclinic crystals of *T. cruzi* GAPDH contain one tetramer per asymmetric unit. The subunits were independently refined, allowing a detailed analysis of the local 222 symmetry. Superposition of Cα atoms from equivalent domains in each pair of subunits in the enzyme (Table 3) clearly shows that the catalytic domains are much more similar than the NAD binding domains, which is analogous to what was observed by Skarzynski et al. (*Bacillus stearothermophilus*) (*16*). This reflects the functionally important flexibility of the coenzyme binding domain needed to allow the rapid exchange of NAD in reduced and oxidized states during catalysis. Indeed, the structure of *T. cruzi* GAPDH complexed with the natural inhibitor chalepin (*42*) shows a large conformational change of the coenzyme binding domain, mainly described as a domain rotation of ∼4°. Also, in that report, only one monomer of the enzyme in the crystal has an observable bound inhibitor. Likewise, in the structure presented here, we find asymmetric binding of the inhibitor and cofactor to the four independent subunits of the enzyme. This observation suggests that in solution the enzyme−inhibitor complexes have a distribution of

populations with different numbers of subunits occupied by the inhibitor, resulting in asymmetric particles which are subsequently selected by the crystallization process, to predominantly accommodate one particular conformer in the crystal lattice. Furthermore, this finding of alternative conformations for the bound inhibitor suggests that **3c** has extended flexibility in the active site, which may also explain the absence of observable connected electron density in the Fourier maps of subunit A.

The comparison of the structure presented here with those of *T. cruzi* GAPDH in the holo form (*22*) and apo form complexed with the natural product inhibitor chalepin (*42*) indicates that the major changes are related to the orientation of Arg249. In Souza et al. (*22*) and Pavão et al. (*42*), where no phosphate ion or substrate analogue is present in the active site of *T. cruzi* GAPDH, Arg249 points to Asp210. In the **3c**−gGAPDH complex, this residue points to Thr197 and Thr199 and hydrogen bonds to phosphate groups both in P_s and P_i conformations (Figure 2A,B). Another interesting feature is the distance between Nϵ of His194 and Sδ of Cys166, which ranges from 3.2 Å in the holo structure to 3.7 Å in the apo structure. In our structure, this distance ranges from 4.1 to 4.4 Å. The longer distance may be a consequence of **3c** binding to the P_i binding site. All other residues in the vicinity of the active site do not present significant side chain displacement, apart from the loop from Ser224 to Ala229, which has its Cα atoms displaced toward the P_i binding site by 0.55 Å, although side chain conformations remain unchanged. Similar behavior was previously reported in the crystallographic structure of *L. mexicana* gGAPDH, crystallized at low $(NH_4)_2SO_4$ concentrations (*41*), and in the hemiacetal intermediate of *E. coli* GAPDH (*24*).

DISCUSSION

Thioacyl Enzyme-Induced Structural Changes. Analysis of differences between the structure of apo- and holo-GAPDH (*16*) confirms the conformational changes in the enzyme induced by cofactor binding. In addition to the coenzyme binding domain, the most significant of these structural changes involves the segment of polypeptide chain spanning residues 224−229. This portion of the backbone, which includes Thr226, contributes to the building of the P_i site, and a small change in the shape of this fragment is essential for the formation of an effective P_i site. Comparison of the distances between the main chain atoms of this loop portion for the holo form of *T. cruzi* gGAPDH (*22*) and the holo-thioacyl enzyme form (monomers B−D) reveals that the corresponding segment moves closer to the P_i binding site in the holo-thioacyl enzyme. Thus, the distance between the P_i and this loop decreases to 0.55 Å. The same conformational change was observed in the crystallographic structure of the apothiohemiacetal enzyme of *E. coli* GAPDH (*24*) (residues 207−212) but to a lesser extent since NAD^+ is not present. This experimental evidence suggests that the widest protein deformation amplitude is observed in the ternary complex in which the GAP induces an essential conformational change leading to the catalytic structure and not only by NAD^+ binding. As for many other enzymes, the productive conformation is obtained by cofactor binding (here NAD^+, ATP for kinases) and also by substrate binding.

GAP Binding P_i Site. When the GAP analogue is bound at the P_i site, the interaction between the carbonyl of the thioester group and the positively charged nitrogen of the nicotinamide ring of NAD^+ is evidenced in the holo-thioacyl enzyme crystallographic structure. A similar interaction was proposed in the hemiacetal enzyme (*24*) of *E. coli* GAPDH in the model built by implementation of the NAD^+ unit in the X-ray structure. On the basis of this model, Park et al. (*24*) proposed that the GAP's phosphate moiety would be displaced from the P_i to the P_s site through a rotation of the C1−C2 covalent bond. Our results with the holo-acyl enzyme complex (Figure 3) suggest a different situation (see below).

GAP Binding P_s Site. The X-ray structure reveals two major points regarding the P_s binding site. First, it is strictly defined and more specific in space than the P_i site, as shown in *B. stearothermophilus* (*16*). This statement is corroborated by minor P_s site position displacement in the **3c**−gGAPDH complex when compared to the *L. mexicana* (0.93 Å) (*41*) and *T. brucei* (0.70 Å) (*17*) structures (Figure 2B). Second, the flipping of the phosphoryl group occurs through a rotation around the cysteine sulfur atom−C1 bond and not around the C1−C2 bond as proposed by Park et al. for the hemiacetal intermediate through the modeling study. This is clearly ilustrated in Figure 3.

Mechanistic Aspects. Although compound **3c** is not equivalent to GAP (absence of a hydroxyl group at C2 and the oxygen linked to the phosphorus is replaced with a carbon), the similarity, particularly in terms of chain length, is sufficiently good to gain additional clarification on the situation of the actual thioester intermediate. Compound **3c** binds to the essential cyteine as does GAP, and the distance between the sulfur atom of Cys166 and the phosphorus atom is the same in both compounds, a point which is essential in a discussion of the interactions of the phosphorus with the P_i and P_s sites.

The thioester intermediate obtained in the presence of NAD^+ gives a structure very close to that required for catalytic efficiency and provides evidence that after covalent binding, GAP induces an additional conformational change. The overall structure shows a major significant structural difference between the P_i and P_s binding sites: the rather flexible position of the P_i site, which does not justify the possibility of a new P_i binding site in the case of *Leishmania* and *E. coli* GAPDH, in contrast to the rather restricted situation of the P_s binding site, at least as revealed from three different GAPDHs.

Our results are compatible with the currently accepted catalytic mechanism. Without ligand (monomer A), Cys166 points toward His194, with the S−H group in a favorable orientation for the transfer of its proton to the histidine acceptor. The nucleophile being formed at sulfur can then attack C1 of the substrate to form the thiohemiacetal intermediate, followed by the hydride ion transfer from C1 to NAD leading to the formation of the thioester, represented in our case by the **3c** P_i conformation; His194, still protonated, is far from the S−C1 bond (~4.6 Å). Following the P_i−P_s exchange, represented in our case by the **3c** P_s conformation, there is a considerable approximation of the carbonyl of the ligand to His194, which is now in a favorable position for mediating the back transfer of the proton to Cys166, completing the reaction cycle.

These results give support to the flip-flop mechanism since the same covalent intermediate can bind either to the P_i site or to the P_s site as seen in subunits B and C (Figure 1B shows **3c** in subunit B). Although largely anticipated by previous authors (*16*, *23*) and in agreement with the results of other authors (*24*), the proposed flip-flop mechanism, through a conformational isomerization step, would occur before the phosphorylation step and would take place during coenzyme exchange. The crystal structure of the holothioacyl gGAPDH complex supports the idea that this flip-flop is likely related to the cofactor exchange process. An alternative interpretation where the characterized P_s site would be the only one representative of the true complex formed with D-GAP, whereas the identified P_i site would be one among several possibilities, seems unlikely. Indeed, localization of the P_i site obtained from the X-ray structure presented here is in agreement with other catalytic features.

In the P_i conformation, as underlined above, there is a strong interaction between the carbonyl group of the thioester and the nicotinamidium ring. However, in the P_s conformation (at this stage, the cofactor is in its reduced form), the carbonyl group−NADH ring distance increases, weakening the corresponding interaction facilitating cofactor release. Likewise, Arg249 may play a major role in this isomerization step. In fact, in the absence of substrate, Arg249 makes a salt bridge with Asp210 (*22*), but when the substrate is present, Arg249 becomes essential at the P_s site and is 5.02 Å from the initial position. One interesting aspect of our structure is the participation of Arg249 in the phosphate coordination in both P_i and P_s conformers. In the P_i conformation, Arg249 binds to the phosphate through the Nδ atom, whereas in the P_i conformation, the binding is through Nη of the guanidinium moiety. Previously, Arg249 was supposed to be composed of only the P_s binding site, and its function in product release was also surmised on the basis of the large conformational change observed in ion free *T. cruzi* GAPDH structures (*22*).

Further important evidence comes from the comparison of partial NAD^+ occupation in monomers B and C (both conformations) and full occupation in monomomer D (P_s conformation only), which strongly suggests that the presence of NAD^+ is related to the P_s conformation. This might be a consequence of hydrogen bond stabilization due to phosphate group interaction with the ribose sugar of the coenzyme, possibly in either the oxidized or reduced cofactor states, as well as hydrophobic contacts between GAP and NAD^+.

The mechanistic steps highlighted by the crystallographic structure can be summed up as follows:

(i) GAP binds to the P_i binding site, positioning the carbonyl group to interact with the positively charged nicotinamidium ring.

(ii) Hydrogen transfer to cofactor leads to a loss of charge interaction and displacement of the reduced cofactor.

(iii) The thioacyl intermediate flips to the P_s binding site, and a new NAD^+ molecule is now stabilized through hydrogen bonding of the phosphate to ribose and hydrophobic contacts.

The results that we obtained with a close analogue of the thioester intermediate formed between GAPDH and its substrate, more precisely the analysis of the interactions of the two alternative conformations found in the crystal, provide a complementary piece of evidence for this sequence.

SUPPORTING INFORMATION AVAILABLE

Synthetic strategy for compounds **1c** and **2c** (Scheme 1) and **3c** (Scheme 2) and detailed synthetic procedures for compounds **1c** and **2c**. This material is available free of charge via the Internet at http://pubs.acs.org.

REFERENCES

1. Sirover, M. A. (1999) *Biochim. Biophys. Acta 1432*, 159−184.
2. Sunaga, K., Takahashi, H., Chuang, D. M., and Ishitani, R. (1995) *Neurosci. Lett. 200*, 133−136.
3. Schulze, H., Schuyler, A., Stuber, D., Dobeli, H., Langen, H., and Huber, G. J. (1993) *Neurochem. 60*, 1915−1922.
4. Burke, J. R., Enghild, J. J., Martin, M. E., Jou, Y. S., Myers, R. M., Roses, A. D., Vance, J. M., and Strittmatter, W. J (1996) *Nat. Med. 2*, 347−350.
5. Koshy, B., Matilla, T., Burright, E. N., Merry, D. E., Fischbeck, K. H., Orr, H. T., and Zoghbi, H. Y. (1996) *Hum. Mol. Genet. 5*, 1311−1318.
6. Epner, D. E., Partin, A. W., Schalken, J. A., Issacs, J. T., and Coffey, D. S. (1993) *Cancer Res. 53*, 1995−1997.
7. Bakker, B. M., Michels, P. A. M., Opperdoes, F. R., and Westerhoff, H. V. (1999) *J. Biol. Chem. 274* (21), 14551−14559.
8. Bressi, J. C., Verlinde, C. L. M. J., Aronov, A. M., Le Shaw, M., Shin, S. S., Nguyen, L. N., Suresh, S., Buckner, F. S., Van Voorhis, W. C., Kuntz, I. D., Hol, W. G. J., and Gelb, M. H. (2001) *J. Med. Chem. 44*, 2080−2093.
9. Engel, J. C., Franke de Cazzulo, B. M., Stoppani, A. O., Cannatta, J. J., and Cazzullo, J. J. (1987) *Mol. Biochem. Parasitol. 26*, 1−10.
10. Duggleby, R. G., and Dennis, D. T. (1974) *J. Biol. Chem. 249*, 167−174.
11. Harrigan, P. J., and Trentham, D. R. (1973) *Biochem. J. 135*, 695−703.
12. Segal, H. L., and Boyer, P. D. (1953) *J. Biol. Chem. 204*, 265−281.
13. Harris, J. I., and Watres, M. (1976) in *The Enzymes* (Boyer, P. D., Ed.) Vol. 13, pp 1−49, Academic Press, New York.
14. Watson, H. C., Duée, E., and Mercer, W. D. (1972) *Nat. New Biol. 240*, 130.
15. Moras, D., Olsen, K. W., Sabesan, M. N., Buehner, M., Ford, G. C., and Rossmann, M. G. (1975) *J. Biol. Chem. 250*, 9137−9162.
16. Skarzynski, T., Moody, P. C. E., and Wonacott, A. J. (1987) *J. Mol. Biol. 193*, 171−187.
17. Vellieux, F. M. D., Hajdu, J., Verlinde, C. L. M. J., Groendijk, H., Read, R. J., Greenhough, T. J., Campbell, J. W., Kalk, K. H., Littlechild, J. A., Watson, H. C., and Hol, W. G. J. (1993) *Proc. Natl. Acad. Sci. U.S.A. 20*, 2355−2359.
18. Tanner, J., Hecht, R. M., Pisegna, M., Seth, D. M., and Krause, K. L. (1994) *Acta Crystallogr. D50*, 744−748.
19. Korndörfer, I., Steipe, B., Huber, R., Tornschy, A., and Jaenicke, R. (1995) *J. Mol. Biol. 246*, 511−521.
20. Kim, H., Feil, I. K., Verlinde, C. L. M., Petra, P. H., and Hol, W. G. J. (1995) *Biochemistry 34*, 14975−14986.
21. Duée, E., Olivier-Deyris, L., Fanchon, E., Corbier, C., Branlant, G., and Dideberg, O. (1996) *J. Mol. Biol. 257*, 814−838.
22. Souza, D. H. F., Garratt, R. C., Araùjo, A. P. U., Guimarães, B. G., Jesus, W. D. P., Michels, P. A. M., Hannaert, V., and Oliva, G. (1998) *FEBS Lett. 424*, 131−135.
23. Corbier, C., Michels, S., Wonacott, A. J., and Branlant, G. (1994) *Biochemistry 33*, 3260−3265.
24. Yun, M., Park, C. G., Kim, J. Y., and Park, H. W. (2000) *Biochemistry 39*, 10702−10710.
25. McCaul, S., and Byers, L. D. (1976) *Biochem. Biophys. Res. Commun. 72*, 1028−1032.
26. Cane, D. E., and Sohng, J. K. (1989) *Arch. Biochem. Biophys. 270*, 50−54.
27. Lambeir, A. M., Loiseau, A. M., Kuntz, D. A., Vellieux, F. M., Michels, P. A. M., and Opperdoes, F. R. (1991) *Eur. J. Biochem. 198*, 429−436.
28. Sakai, K. J., Hasumi, K., and Endo, A. (1991) *Biochim. Biophys. Acta 1077*, 192−199.
29. Willson, M., Lauth, N., Périé, J., Callens, M., and Opperdoes, F. R. (1994) *Biochemistry 33*, 214−220.

30. Cane, D. E., and Sohng, J. K. (1994) *Biochemistry 33*, 6524−6530.
31. Polikarpov, I., Perles, L. A., de Oliveira, R. T., Oliva, G., Castellano, E. E., Garratt, R. C., and Craievich, A. (1998) *J. Synchrotron Radiat. 5*, 72−76.
32. Arndt, U. W., and Wonacott, A. J. (1997) *The rotation methods in crystallography*, North-Holland Publishing Co., Amsterdam.
33. Otwinowski, Z., and Minor, W. (1997) *Methods Enzymol. 276*, 307−326.
34. Navaza, J. (1994) *Acta Crystallogr. A50*, 157−163.
35. Brunger, A. T., Adams, P. D., Clore, G. M., Delano, W. L., Gros, P., Grosse-Kunstleve, R. W., Jiang, J.-S., Kuszewski, J., Nilges, M., Pannu, N. S., Read, R. J., Rice, L. M., Simonson, T., and Warren, G. L. (1998) *Acta Crystallogr. D54*, 905−921.
36. Lamzin, V. S., and Wilson, K. S. (1993) *Acta Crystallogr. D49*, 129−147.
37. Jones, T. A., Zou, J. Y., Cowan, S. W., and Kjeldgaard, M. (1991) *Acta Crystallogr. A47*, 110−119.
38. Laskowski, R. A., Macarthur, M. W., Moss, D. S., and Thorton, J. M. (1993) *J. Appl. Crystallogr. 26*, 283−291.
39. Meloche, H. P. (1967) *Biochemistry 6*, 2273−2276.
40. Ramachandran, G. N., Ramakrishnar, C., and Sasisekhran, V. (1963) *J. Mol. Biol. 7*, 95−99.
41. Kim, H., and Hol, W. G. (1998) *J. Mol. Biol. 278*, 5−11.
42. Pavao, F., Castilho, M. S., Pupo, M. T., Dias, R. L. A., Correa, A. G., Fernandes, J. B., Da Silva, M. F. G. F., Mafezoli, J., Vieira, P. C., and Oliva, G. (2002) *FEBS Lett. 520* (1−3), 13−17.

BI0206107